



Article

Wideband Patch Antenna with Modified L-Probe Feeding for mmWave 5G Mobile Applications

Woncheol Lee ^{1,2}, Hoyun Won ¹, Yang-Ki Hong ^{1,*}, Minyeong Choi ¹ and Sung-Yong An ³

- Department of Electrical and Computer Engineering, The University of Alabama, Tuscaloosa, AL 35487, USA; woncheol.lee@samsung.com (W.L.); hwon@crimson.ua.edu (H.W.); mchoil1@hyundai.com (M.C.)
- ² RF Development Team, S.LSI, Samsung Electronics, Hwaseong 18448, Republic of Korea
- Corporate R&D Institute, Samsung Electro-Mechanics Co., Ltd., Suwon 16674, Republic of Korea; sung.an@samsung.com
- * Correspondence: ykhong@eng.ua.edu

Abstract: This paper presents a wideband low-profile dual-polarized patch antenna with helical-shaped L-probe feeding (HLF) for mmWave 5G mobile device applications. Parametric studies on the HLF structure are performed to identify the optimal specifications. As a result, the optimized antenna achieves a wide bandwidth of 5.4 GHz (24.2–29.6 GHz), good isolation > 18 dB between ports, and 5.1 dBi of good peak realized gain, which is experimentally verified with a $10\times$ upscaled antenna. In addition, various one \times four phased arrays with different port configurations and beamform capabilities are designed and simulated for the peak realized gain. The designed antenna array shows a high peak realized gain of 10 dBi, high isolation of 15 dB between the ports, and a small substrate thickness of $0.048\lambda_0$ (λ_0 is the wavelength of 24.25 GHz). Compared to the state-of-the-art antennas, the designed dual-polarized antenna can operate in the frequency ranges of 24.25–29.6 GHz, including n257, n258, and n261 of the 5G new radio frequency range 2.

Keywords: wideband; patch antenna; L-probe; mmWave; 5G; proximity coupled feeding



Citation: Lee, W.; Won, H.; Hong, Y.-K.; Choi, M.; An, S.-Y. Wideband Patch Antenna with Modified L-Probe Feeding for mmWave 5G Mobile Applications. *Electronics* **2024**, *13*, 3119. https://doi.org/10.3390/ electronics13163119

Received: 10 July 2024 Revised: 2 August 2024 Accepted: 5 August 2024 Published: 7 August 2024



Copyright: © 2024 by the authors. Licensee MDPI, Basel, Switzerland. This article is an open access article distributed under the terms and conditions of the Creative Commons Attribution (CC BY) license (https://creativecommons.org/licenses/by/4.0/).

1. Introduction

The advent of fifth-generation (5G) wireless communication technologies has sparked considerable interest across various applications, enabling ultra-fast data transfer, high-definition video live streaming, and the Internet of Things (IoT) [1]. Critical to supporting these technologies are high data rates, ultra-low end-to-end latency, and high capacity. Leveraging millimeter-wave (mmWave) frequency bands has become pivotal given their broader bandwidth compared to 4G wireless frequency bands. Consequently, many countries have already allocated frequency ranges from 24.25 to 29.5 GHz for 5G networks (low-band: n257, n258, and n261 of 5G new radio (NR) frequency range 2 (FR2)), as shown in Figure 1.

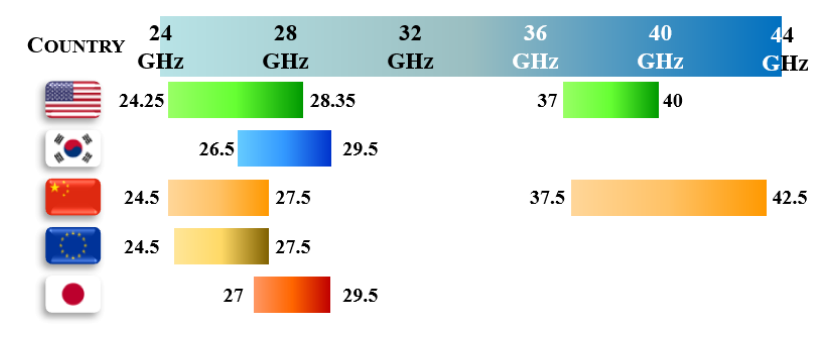


Figure 1. The 5G frequency band allocations across the world in millimeter wave bands [1].

Although mmWave frequency bands offer broad bandwidth, higher frequency bands lead to increased free space path loss. This phenomenon shortens the traveling distance of electromagnetic waves, necessitating a compensatory increase in effective isotropic radiated power (EIRP) to mitigate the effects of increased free space path loss. In response to the need, a high antenna gain is demanded in mmWave wireless communication systems. Antenna arrays, comprised of multiple antenna elements spaced at optimal distances, are deployed to enhance antenna directivity and gain. Nonetheless, the increased directivity of the antenna poses challenges in achieving sufficient wireless communication coverage. Electrical beamforming effectively extends the coverage range to overcome this issue, addressing the challenge.

Recently, antenna-in-package (AiP) technology has emerged, integrating antenna arrays into packages alongside radio-frequency integrated circuits (RFICs). The AiP technology offers several advantages, including low insertion loss by shortening the RF signal path, compactness, fabrication reliability, and cost-effectiveness [2]. Millimeter wave-phased array microstrip antennas have been studied for 5G wireless communication bands. However, conventional microstrip antennas suffer from narrow impedance bandwidth and low gain. To address these issues, various methods, such as loading different substrates [3,4], using an air cavity and glass as substrates [3,5], loading metasurfaces [6], employing an L-shaped probe [7], and loading patterned slots [6], have been proposed. Gu et al. reported a multi-stacked organic- and air cavity-based AiP [3]. The hybrid multilayered method achieves a bandwidth of 3.7 GHz (26.3–30 GHz), but it has issues such as low gain, thick thickness, and limited bandwidth. It does not cover the entire low band of 5G NR FR2. Other reported methods also have problems like low gain, high profile, single polarization, or low operating bandwidth [3–20]. There is a pressing need for a specific technique to effectively address these issues.

This paper introduces a new wideband dual-polarized patch antenna and antenna array that covers n257, n258, and n261 of 5G NR FR2, spanning from 24.25 to 29.5 GHz. The antenna offers high isolation between ports and high gain. Experimental results confirm the simulated performance of this antenna array. A novel helical-shaped L-probe feeding (HLF) structure is introduced to achieve high bandwidth with a low profile.

This paper consists of five sections. Section 2 describes the designed AiP with the HLF. The antenna performance of the AiP is investigated in Section 3. The experimental verification of the $10\times$ upscaled AiP is presented in Section 4. Section 5 covers the design of the 1×4 array and compares the antenna array performance among state-of-the-art antenna designs. Lastly, Section 6 provides concluding remarks.

2. Antenna-in-Package Structure

Figure 2 shows the designed geometry and dimensions of a dual-polarized HLF patch antenna (HLF-PA). The antenna was designed on multilayer laminated FR-4 printed circuit board (PCB) substrates. The measured dielectric constant (ε_r) and dielectric loss tangent (tan δ_ε) of the multilayer laminated FR-4 substrate are 4.02 and 0.018 at 30 GHz, respectively [8]. The stack-up for the antenna consists of a copper-clad laminate (CCL) layer with a thickness (t_{CCL}) of 0.3 mm, 10 layers of prepregs (PPG) with an equal thickness (t_{PPG}) of 60 μ m, and 12 layers of metal with a thickness (t_{Cu}) of 20 μ m, as shown in Figure 2b. Annealed copper is used for all metal layers. The CCL, top five PPGs, and six top-metal (TM) layers are used for the patch antenna structure (antenna portion in AiP). BM1 is the main ground for the patch antenna, and the total thickness of the antenna portion is 600 μ m. The bottom five PPGs and six metal (BM) layers are used for the feeding network, digital, and power lines. The RFIC port is connected to the antenna input terminal at BM2 via transitions from BM1 to BM6 without strip lines in antenna performance simulation [2].

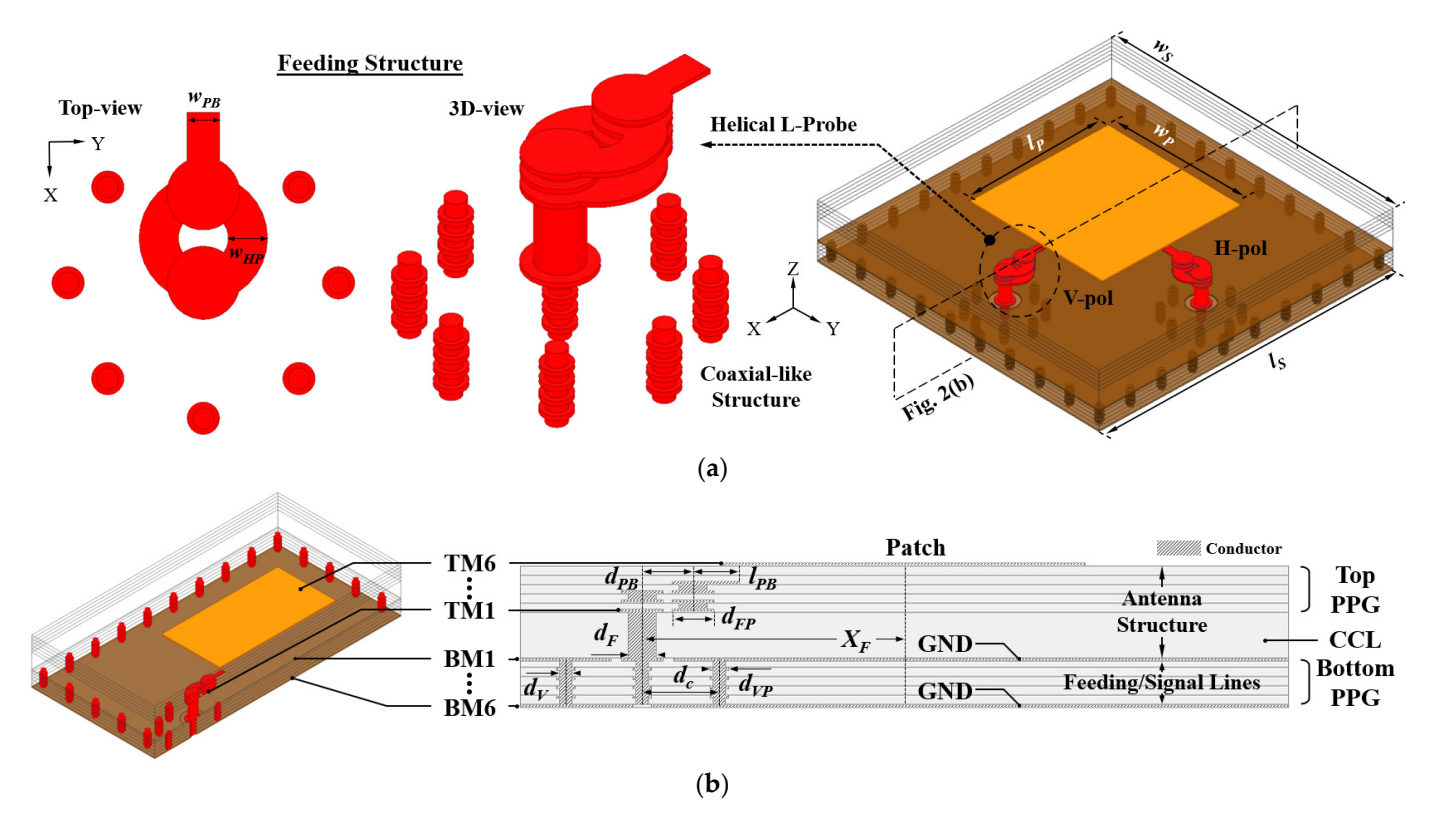


Figure 2. Geometry and dimensions of the proposed (a) dual-polarized helical-shaped L-probe fed patch antenna (HLF-PA) and (b) PCB stack-up of the designed HLF-PA.

Furthermore, eight shorting vias from BM1 to BM6 form a coaxial structure to match the impedance [2]. The guided feeding via transitions is connected to the designed HLF structures at BM1. To increase the antenna impedance bandwidth, the helical L-probe feeding structures are located from BM1 to TM4. Lastly, the patch radiator is situated on the TM6 layer. The antenna dimensions are summarized in Table 1. The performance of the designed AiP was simulated with the ANSYS high-frequency structure simulator (HFSS v.18.1). All simulations in this paper were performed on a Dell Precision T5600 workstation having a CPU (Dual Intel Xeon Processor E5-2697 v2—12 core HT, 2.7 GHz turbo) and 128 GB of RAM.

l_S	w_S	l_P	w_P	l_{PB}	w_{PB}	d_F	d_{FP}	d_{PB}
5	5	2.35	2.35	0.3	0.12	0.18	0.27	0.33
w_{HP}	X_F	d_V	d_{VP}	d_c	t_{PPG}	t_{CCL}	t_{Cu}	Unit in
0.145	1 705	0.08	0.12	0.5	0.06	0.3	0.02	mm

Table 1. Dimensions of wideband dual-polarized 5G mmWave patch antenna structure.

3. Performance of Designed Antenna with Parametric Studies

3.1. Conventional L-Probe and Designed Helical-Shaped L-Probe

One well-known method to broaden the bandwidth is the L-probe proximity coupled feeding method, as illustrated in Figure 3a [5,7]. A self-resonance of the feeding structure near the fundamental resonance of the patch antenna can broaden the impedance bandwidth of the L-probe-fed patch antenna [7]. Accordingly, the total length of the L-probe feeding (sum of vertical and horizontal lengths) is an essential parameter in achieving a broad impedance bandwidth. Additionally, the horizontal portion of the conventional L-probe feeding controls the coupling coefficient, i.e., the resonant frequency of the antenna, between the L-probe feeding and the driven patch. Hence, the horizontal portion of the

Electronics **2024**, 13, 3119 4 of 17

L-probe feeding must have an appropriate length and width. Figure 4a shows the simulated scattering parameters (S-parameters) of the conventional L-probe feeding without a patch radiator. The length of the vertical part of the L-probe feeding is 500 μ m in this simulation. The length of the horizontal portion of the L-probe feeding (l_{PB}) varies from 0.9 to 1.5 mm to identify the resonance of the conventional L-probe feeding. As expected, the resonant frequency shifts from 40 to 26 GHz as the l_{PB} increases. When the l_{PB} is 1.5 mm, the L-probe feeding resonates near 27 GHz, close to the center frequency, covering n257, n258, and n261. However, poor isolation between ports is observed in Figure 4a, which is attributed to coupling between ports for V- and H-polarizations. For this reason, the conventional L-probe feeding method is unsuitable for 5G mmWave AiP to realize a broadband dual-polarized antenna.

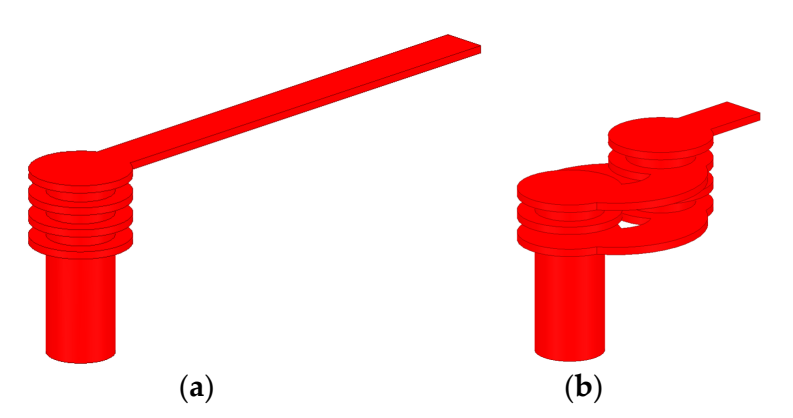


Figure 3. Geometry of **(a)** the conventional L-probe and **(b)** the designed helical-shaped L-probe structure.

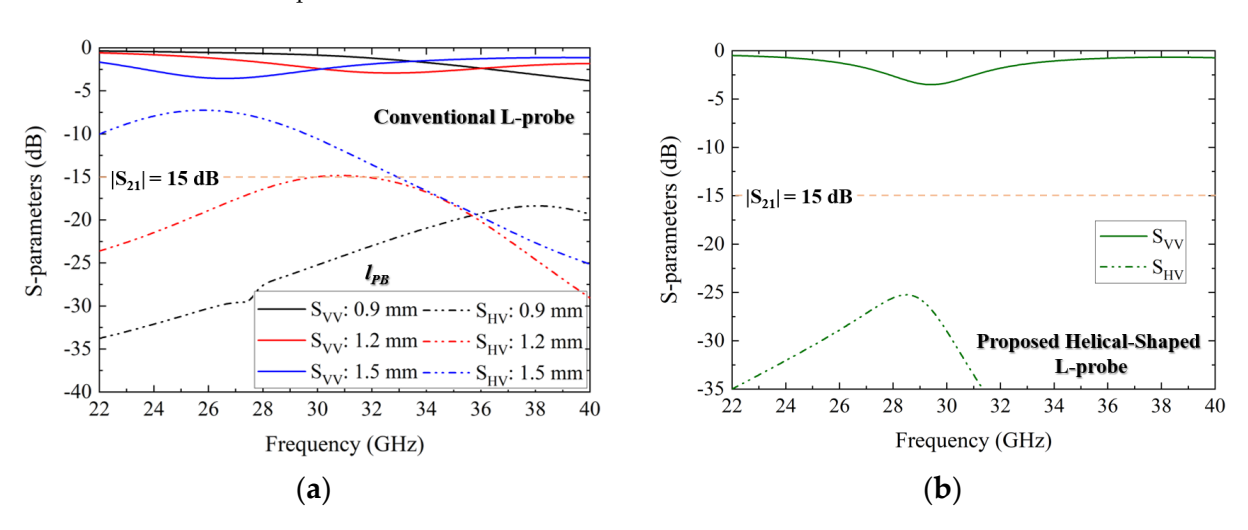


Figure 4. Simulated S-parameters: (a) conventional L-probe with various l_{PB} and (b) designed helical-shaped L-probe without the patch radiator.

To address the issue, the HLF is newly designed, as illustrated in Figure 3b. The designed feeding structure consists of a vertical component, which has a helical winding structure with 1.5 turns that is connected between BM1 through TM3, and a horizontal component located at TM4. The designed structure decreases the l_{PB} of the conventional L-probe-fed antenna by 1.2 mm. The simulated resonant frequency of the designed feeding probe is 29.4 GHz.

Regarding the mutual coupling between V- and H-pol ports, a minimum isolation greater than 25 dB between the two ports is achieved due to the decreased l_{PB} , as shown in Figure 4b. Figure 5a,b show the simulated surface current distribution of the conventional and the designed HLF at 27 GHz, respectively, when Port 1 is excited. At the same time, Port

Electronics **2024**, 13, 3119 5 of 17

2 is terminated with 50 Ω . The simulated surface current distribution shows the improved isolation between the two ports with the HLF structure replaced by the conventional L probe. A strong surface current is observed from the terminated port (Port 2) in a conventional L-probe structure when Port 1 is excited in Figure 5a. On the other hand, the designed HLF structure shows a negligible coupling effect between ports in Figure 5b.

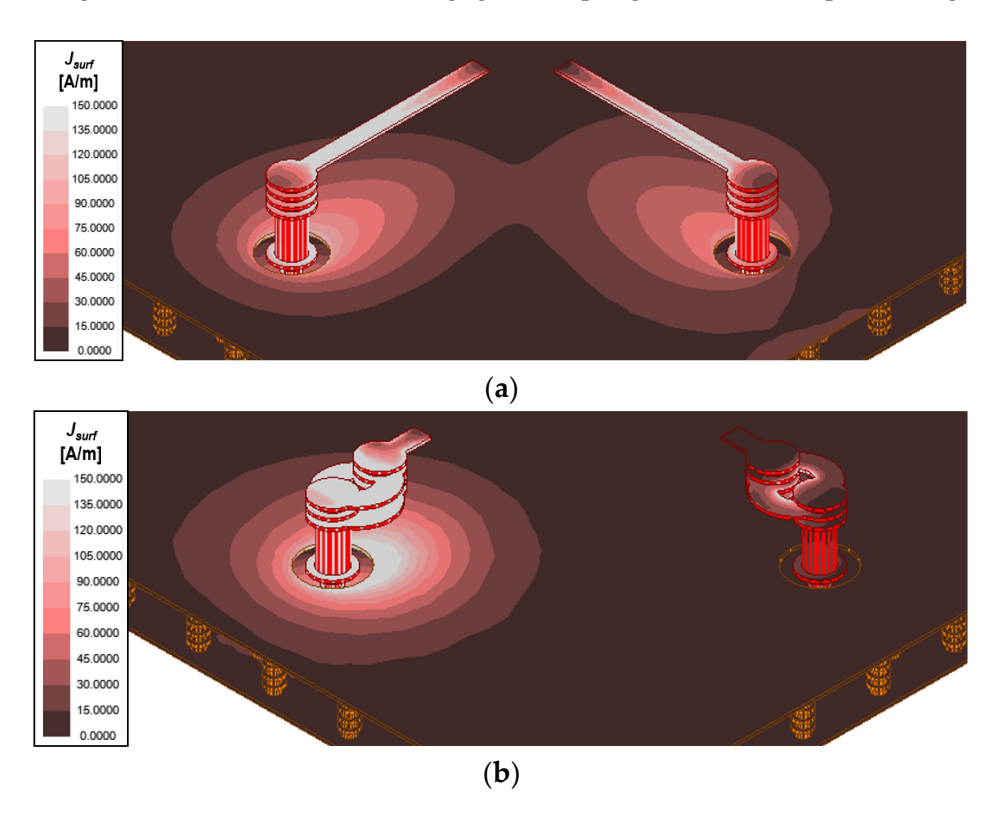


Figure 5. Simulated surface current density distribution of (**a**) the conventional L-probe and (**b**) the designed helical-shaped L-probe without the patch radiator at 27 GHz.

Figure 6 shows the S-parameters of the conventional L-probe and the designed HLF with a patch radiator. The same rectangular patch radiator of TM6 is used for both L-probes. The resonant frequency of 26 GHz without the patch radiator shifts to 30.5 GHz when the patch radiator is introduced on the conventional L-probe. This is mainly attributed to the capacitance (C_{pat_up}) between the upper probe and patch radiator in Figure 7a. The high C_{pat_up} is induced by the coupling between the patch and the conventional L-probe with a longer l_{PB} than the designed L-probe. The feeding position is moved toward the edge of the ground to reduce the coupling, resulting in a larger antenna size. Another method is to shorten the L-probe's vertical length, increasing the gap between the patch radiator and the horizontal portion of the L-probe. However, this approach requires increased laminated PCB thickness, making manufacturing costly and complex. Therefore, both methods are unsuitable for the low-profile broadband dual-polarized patch antenna. In contrast, the designed dual-polarized patch antenna with an HLF shows a good -10 dB impedance bandwidth of 5.4 GHz (24.2–29.6 GHz) with high isolation ($|S_{21}|$) greater than 18 dB. The introduction of L₃, C₂, and C₃ in Figure 7b allows a short horizontal portion of the L-probe feeding. Accordingly, the optimal coupling coefficient and high isolation between V- and H-pol ports can be achieved within the limited size and thickness.

Electronics **2024**, 13, 3119 6 of 17

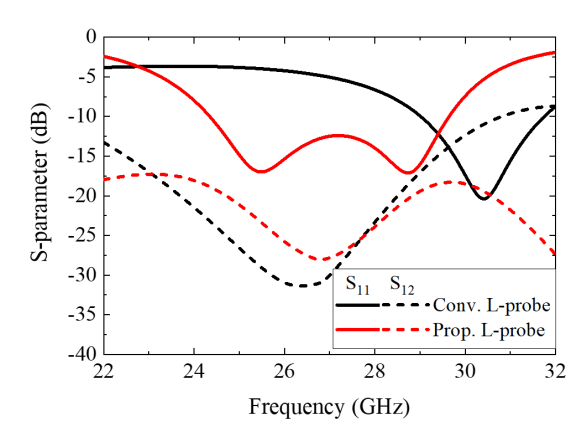


Figure 6. Simulated S-parameters of the conventional L-probe and the designed helical-shaped L-probe with a patch radiator.

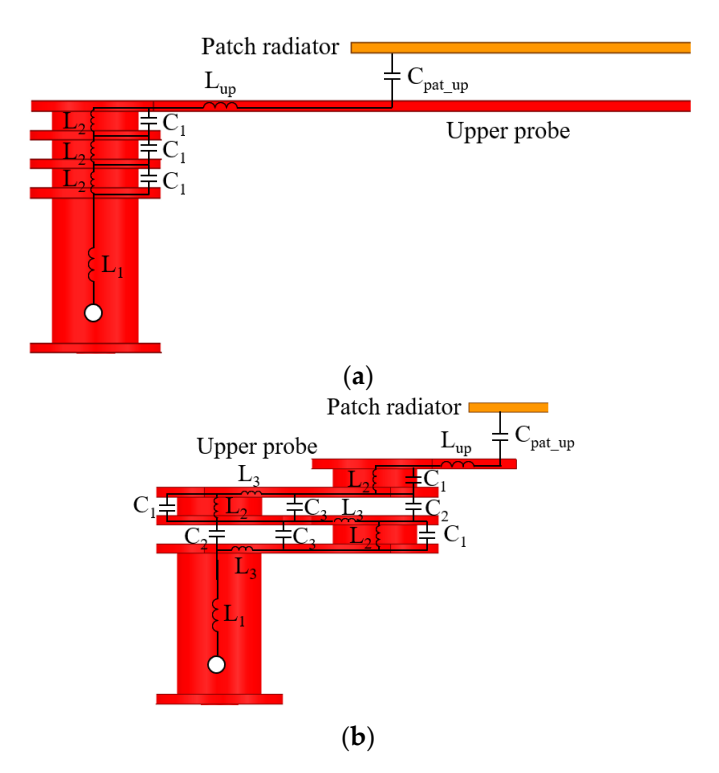


Figure 7. Equivalent circuit of **(a)** the conventional L-probe and **(b)** the designed helical-shaped L-probe.

3.2. Parametric Studies on Various HLF Dimensions

Parametric studies on various HLF dimensions were conducted to analyze the effects on antenna performance, determining the optimal HLF dimensions. First, the reflection and transmission characteristics of the designed HLF are analyzed for various l_{PB} of the HLF structure in Figure 8. As the l_{PB} increases from 0.2 to 0.5 mm, the resonance of the S_{11} shifts from a low to a high frequency. In contrast, the transmission coefficient (S_{21}) is insignificantly affected. Similarly, the resonance of the S_{11} shifts from a low to a high frequency as the width (w_{PB}) increases from 0.06 to 0.24 mm without changing S_{21} , as shown in Figure 9a. The S_{11} degrades from -30 to -10 dB in the frequency range between 25 and 26 GHz, while the S_{11} improves from -12.5 to -40 dB in the frequency ranges between 28.5 and 29 GHz with an increase of w_{PB} .

Electronics **2024**, 13, 3119 7 of 17

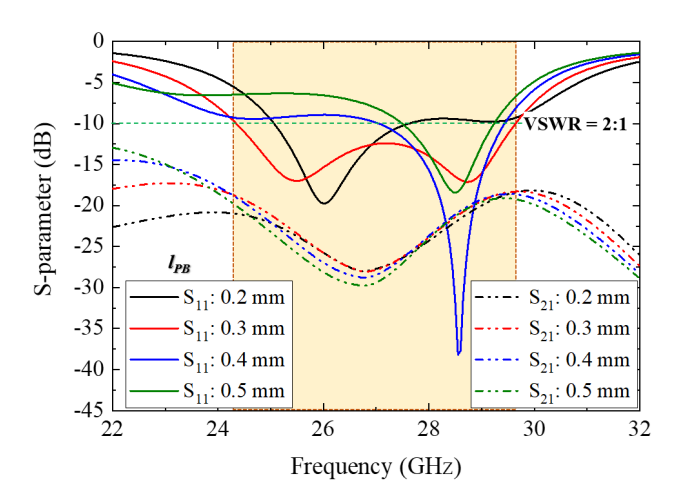


Figure 8. Simulated S-parameters of the designed helical-shaped L-probe with various l_{PB} .

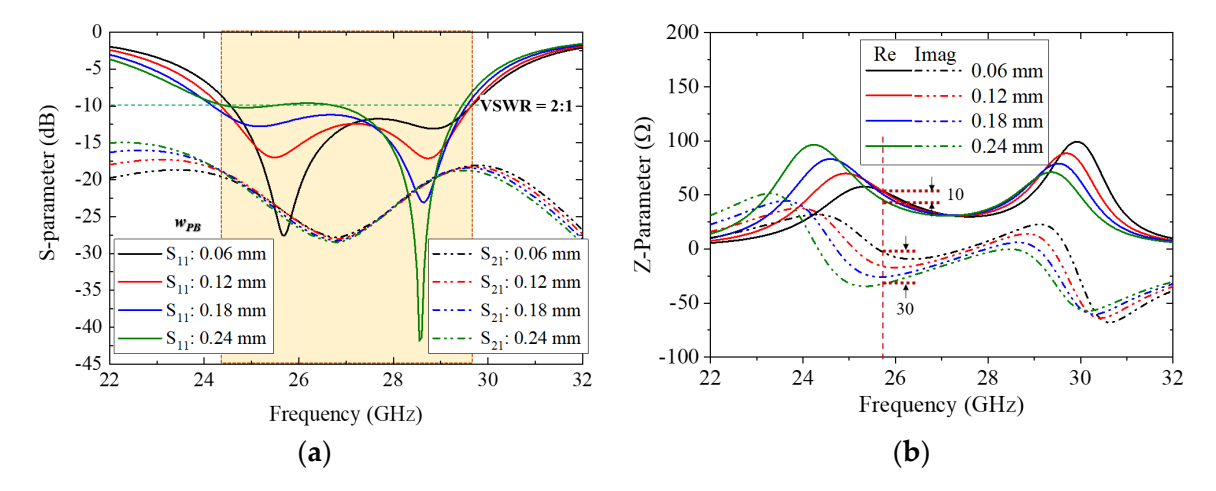


Figure 9. Simulated (a) S- and (b) Z-parameters of the designed helical-shaped L-probe with various w_{PB} in mm.

Antenna input impedance is subject to reactance (Z_{imag}), which is affected by the coupling coefficient between the patch radiator and the horizontal portion of the HLF. Figure 9b shows the simulated resistance and reactance at various w_{PB} values as a function of frequency. The resistance changes within 10 ohms at 25.5 GHz as the w_{PB} varies between 0.06 and 0.24 mm, while the reactance varies within 30 ohms at the same frequency. A l_{PB} of 0.3 mm and w_{PB} of 0.12 mm are chosen for further study, since the antenna with the given dimensions shows good S_{11} and S_{21} in the desired frequency bands.

Figure 10 shows the effects of the distance (X_F) between the center of the rectangular patch radiator and the center of the stacked via in the CCL for HLF on antenna performance. As the X_F decreases from 1.805 to 1.705 mm, the -10 dB impedance bandwidth improves from 4 to 5.2 GHz at the expense of a slightly high S_{21} . However, the impedance matching degrades when X_F decreases from 1.705 to 1.505 mm. Therefore, the optimum value of 1.705 mm is selected for X_F .

Figure 11 shows the S_{11} and S_{21} characteristics of the designed HLF-PA for various diameters of the helical turn (d_{PB}). Good impedance matching is observed in the frequency ranges from 24.2 to 29.6 GHz for a d_{PB} of 0.33 mm. As d_{PB} increases from 0.32 to 0.34 mm, the second resonant frequency (f_2) shifts from low to high, which is attributed to the increase in the L_3 and total length of the HLF. The simulated results indicate that varying d_{PB} can tune f_2 .

Electronics **2024**, 13, 3119 8 of 17

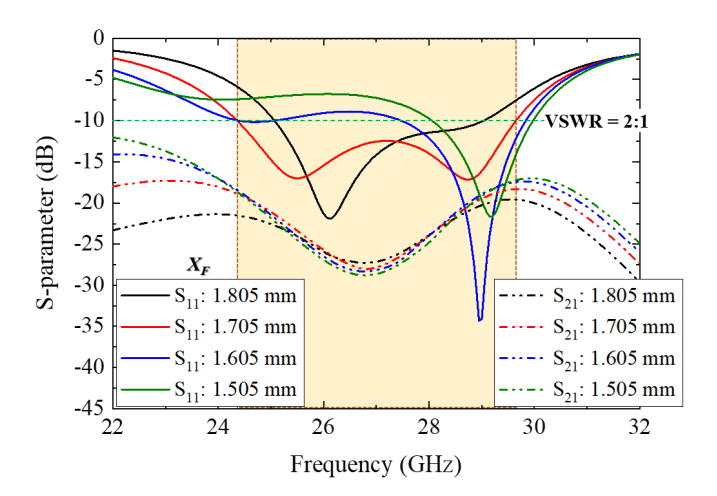


Figure 10. Simulated S-parameters of the designed helical-shaped L-probe with various X_F .

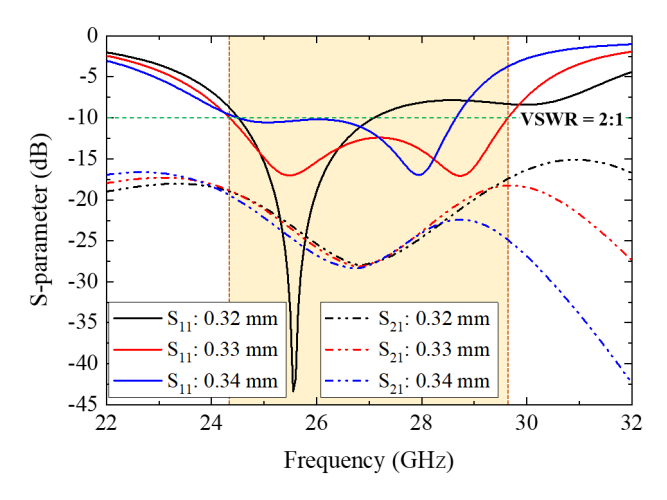


Figure 11. Simulated frequency-dependent S-parameters of the designed helical-shaped L-probe with various d_{PB} .

Figure 12 shows the simulated S-parameter and peak realized gain at boresight (RG₀₀) for the optimized HLF-PA. The HLF-PA shows a wide -10 dB impedance bandwidth of 20% (5.4 GHz: 24.2–29.6 GHz) for both V- and H-pol. High isolation ($|S_{HV}|$) between V- and an H-pol greater than 18 dB is achieved within the frequency bands of interest. The simulated RG₀₀ ranges from 3.7 to 5.1 dBi in the desired operating frequency bands (24.25–29.6 GHz). Figure 13 shows the electric field distribution at 24.25 GHz and 29.5 GHz. As shown, the patch is well excited with the fundamental mode. Figure 14 shows the 2D radiation patterns of the designed HLF-PA at 24.25 GHz and 29.5 GHz. The simulated maximum gains appear at the boresight in the XOZ and YOZ planes, indicating broad-side radiation for both ports. In addition, the co-polarization for V-pol (E_{θ} in the XOZ plane and E_{ϕ} in the YOZ plane) is orthogonal to the co-polarization for H-pol (E_{ϕ} in the XOZ plane and E_{θ} in the YOZ plane) in the same observation plane. Accordingly, the designed HLF-PA exhibits dual-polarization characteristics. Relatively small cross-polarization levels of -20 dB are obtained in the XOZ and YOZ planes.

Electronics **2024**, 13, 3119 9 of 17

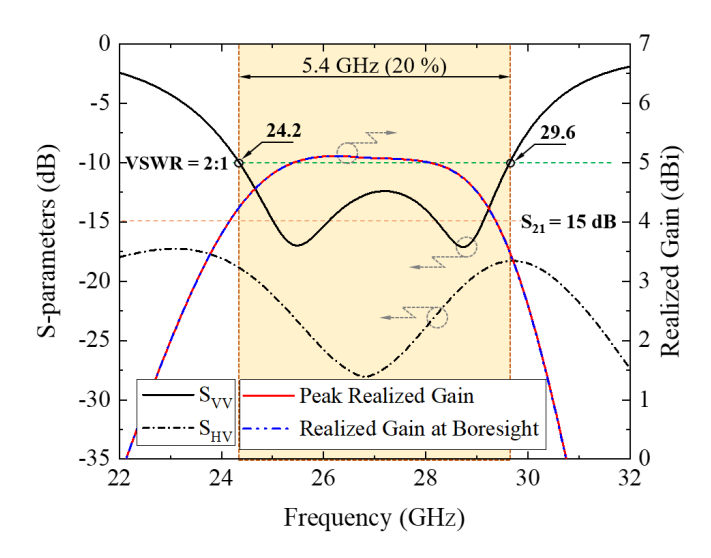


Figure 12. Simulated frequency-dependent S-parameters and peak realized gain at boresight of the designed dual-polarized patch antenna with the helical-shaped L-probe feeding.

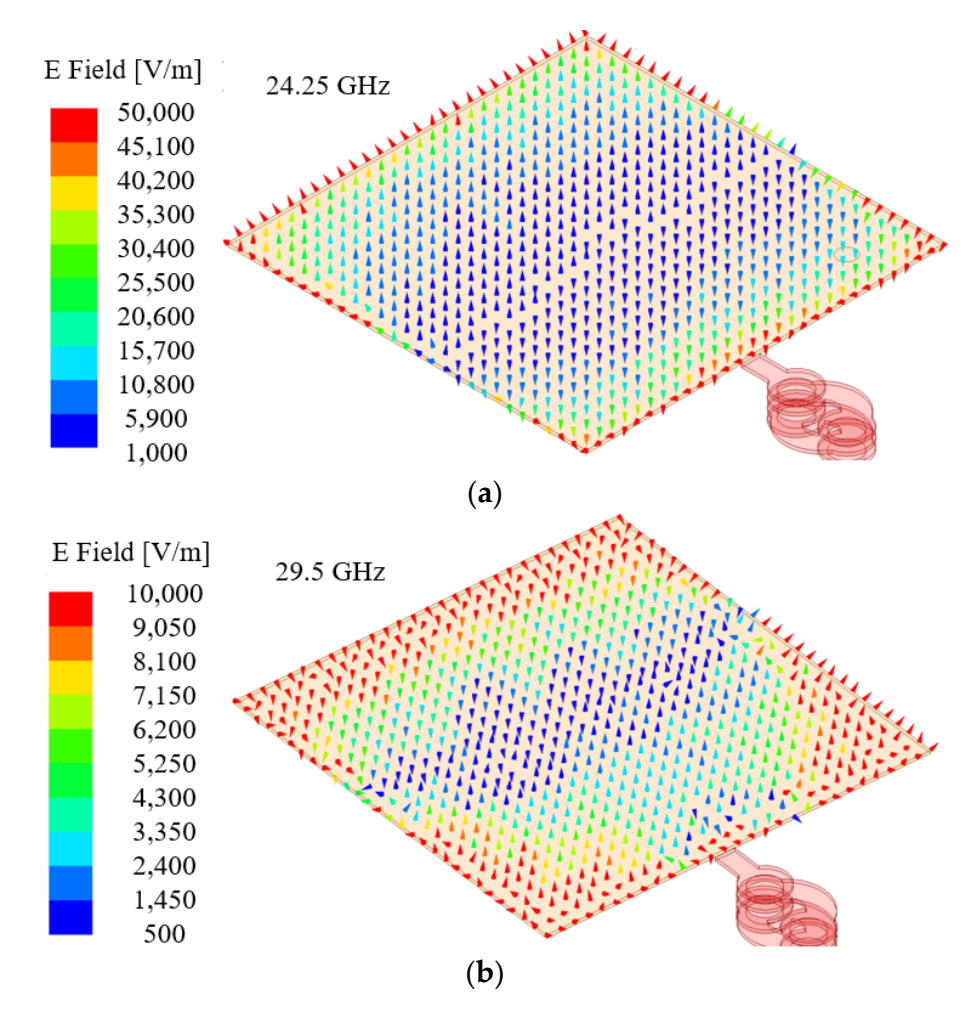


Figure 13. Electric field distribution at (a) 24.25 GHz and (b) 29.5 GHz.

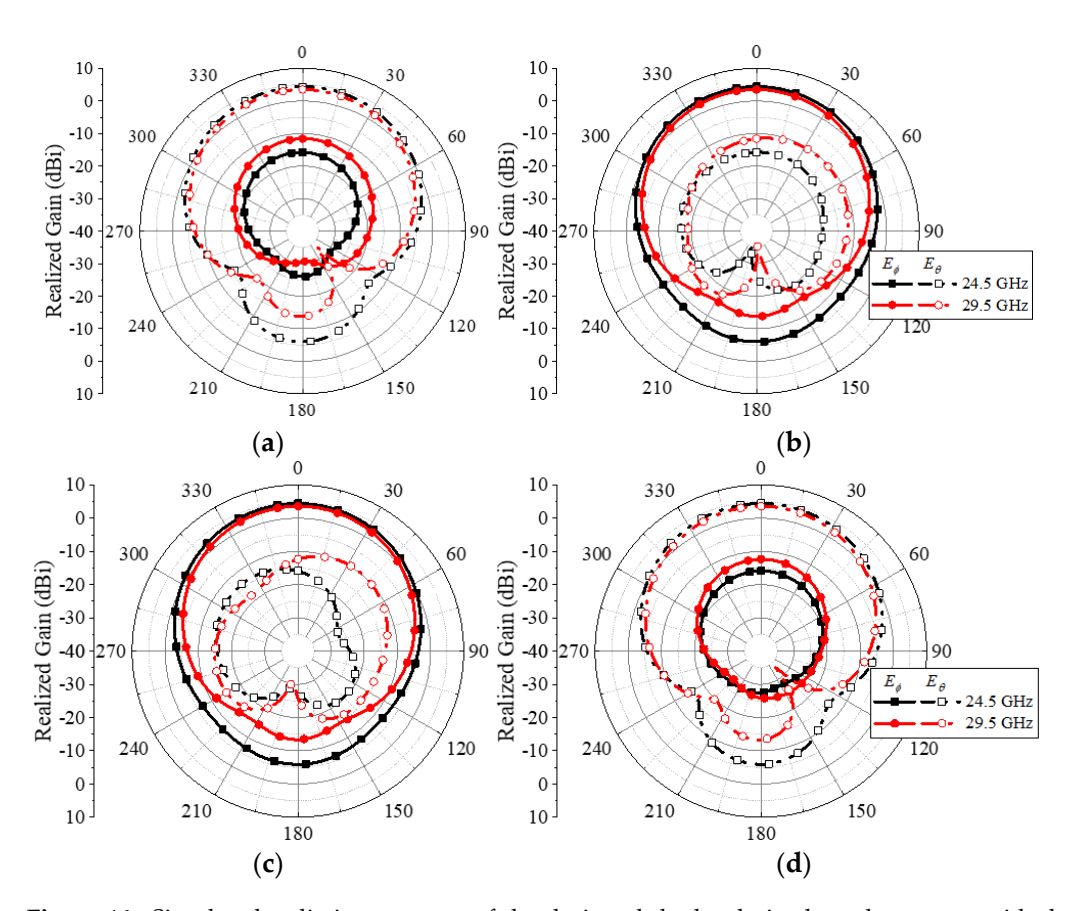


Figure 14. Simulated radiation patterns of the designed dual-polarized patch antenna with the helical-shaped L-probe feeding at 24.5 and 29.5 GHz: V-pol (a) XOZ and (b) YOZ plane and H-pol (c) XOZ and (d) YOZ plane.

4. 10× Upscaled Antenna Experimental Verification

The $10\times$ upscaled proof-of-concept (PoC) antenna is fabricated and characterized to validate the simulated results based on the structural parameters and specifications in Table 1. Since a multilayer PCB with a fine design rule is inaccessible in small quantities, the designed dual-polarized patch antenna with an HLF structure is upscaled ten times for fabrication to validate the proposed concept. Figure 15 shows the fabricated $10\times$ upscaled PoC antenna. An in-house precision milling machine (LPKF ProtoMat S62, LPKF, Garbsen, Germany) is used to mill eight copper layers of double-sided CCL FR-4 epoxy substrates for each layer. Below is the detailed fabrication process.

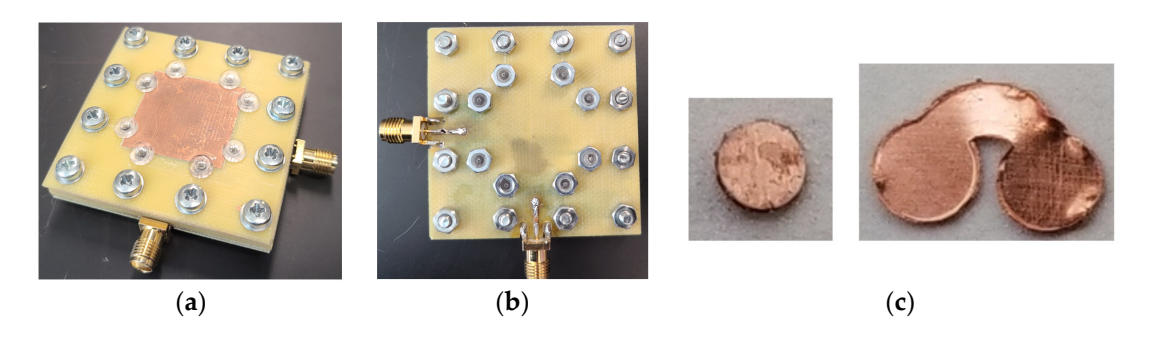


Figure 15. Photo images of the fabricated $10 \times$ upscaled dual-polarized patch antenna with the helical-shaped L-probe: (a) overall, (b) bottom (feeding layer), and (c) parts of helical-shaped L-probe: via (left) and helical-shaped pattern (right). (The 2.92 mm (K-type) connector is suitable for n257, n258, and n261 bands.)

1. To align and fully compress the milled substrates into the antenna using M2.5 \times 10 mm screws and nuts, 2.55 mm diameter holes were punched on the edges of the substrate and copper patch radiator. M2.5 \times 10 mm plastic screws are selected and used on the edge of the copper radiator patch to mitigate the effects of the screws on the radiation from the copper patch radiator.

- 2. The copper foils of FR-4 substrates were milled accordingly for each TM1–TM6, CCL, BM1, and feeding layer. The purpose of the BM layers is to provide feeding between other chipsets. As shown in Figure 15b, the feeding layer replaces these BM layers to ease the fabrication process and feed. The feeding layer thickness is 0.6 mm, and a microstrip line with a width of 1.2 mm and length of 6.8 mm was used to connect with the probe. Then, portions of the FR-4 substrate were milled to provide spaces to embed parts of the proposed HLF structure for the TM1–TM4 and CCL layers.
- 3. The individual parts of the proposed HLF structure used in the TM1 to TM4 layers were punched from a 0.2 mm thick copper sheet, as shown in Figure 15c. The copper rod, with a 1.8 mm diameter, connecting between each TM layer and the TM1 and feeding layers, was cut using a diamond wire saw.
- 4. To integrate the milled substrates and parts of the HLF structure, the FR-4 substrate having the TM1 layer was flipped, and the holes were filled with screws and nuts. After flipping and placing the TM2 layer on top of the TM1 layer, the first copper part of the HLF structure was inserted. Then, the substrate for the TM3 layer was placed on top of the substrate for the TM2 layer. To connect the TM2 and TM3 layers, the copper rod cut in Step 3 was inserted and soldered. Then, the parts for the TM3 layer were included and soldered to connect the copper rod and TM3 layer. This process was repeated to connect the other layers.
- 5. After stacking all substrates, the bolts were tightened to eliminate possible air gaps between the layers. Then, 50 Ω SMA connectors were used to feed the antennas through feeding layers.

The fabricated $10\times$ upscaled PoC antenna was characterized using a vector network analyzer (VNA: Agilent N5230, Agilent, Santa Clara, CA, USA) for S-parameters and an in-house anechoic chamber (Raymond Quietbox AVS 700, Raymond RF, Cleveland, OH, USA) for radiation patterns and realized gain. The antenna was re-simulated with the upscaled dimensions, modified stack-up, and modified feeding structure to compare the measured and simulated results.

Figure 16 shows the simulated and measured S-parameters and RG_{00} of the fabricated $10\times$ upscaled PoC antenna. As depicted in Figure 16a, the HLF-PA shows a wide -10 dB impedance bandwidth of 20% (540 MHz: 2.42 GHz~2.96 GHz) for V-pol and 22.7% (620 MHz: 2.42 GHz~3.04 GHz) for H-pol. Further, the high measured $|S_{21}|$ of greater than 18.2 dB is observed. Measured RG_{00} ranges from 4.0 to 5.2 dBi, closely following the simulated results within ± 0.5 dBi, which is approximately the measurement accuracy of the anechoic chamber. Good agreement between the simulated and measured results is observed. Due to the same simulated S_{11} and S_{22} values, the solid blue line (S_{22}) covers the solid black line (S_{11}) . Small discrepancies between the results may be attributed to minor fabrication errors, frequency-dependent material characteristics, and characterization inaccuracies.

Figure 17 shows the simulated and measured normalized radiation patterns in the E-plane at 2.5, 2.7, and 2.9 GHz for both ports. The measured E-planes show the broadside radiation pattern. The cross-polarization levels are also lower than 15 dB for both ports at all frequencies. These measured results validate the effectiveness of the novel helical L-shaped feeding structure in developing an antenna for 5G mobile devices.

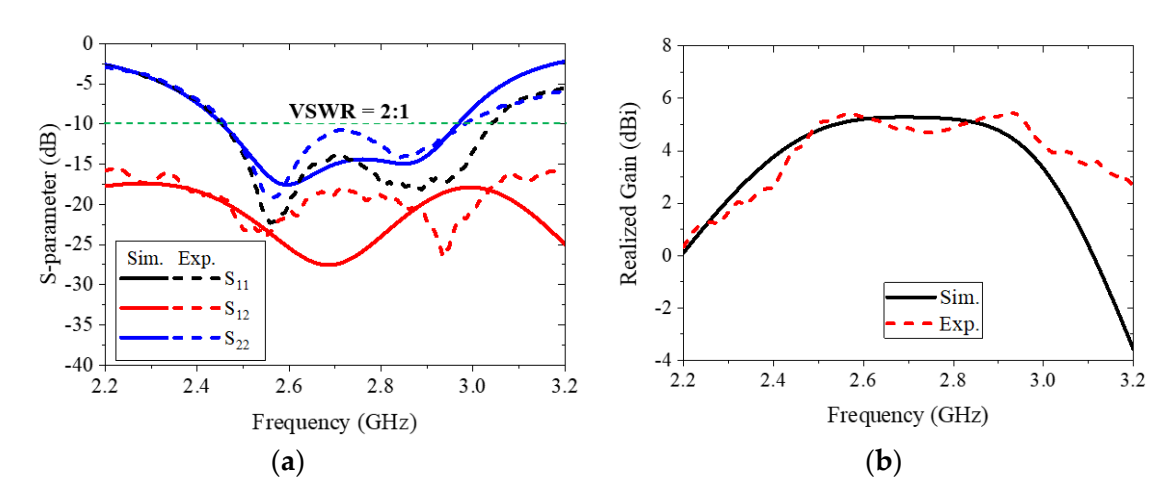


Figure 16. Simulated and measured (a) S-parameters and (b) peak realized gain of the $10 \times$ upscaled fabricated dual-polarized patch antenna with modified L-probe.

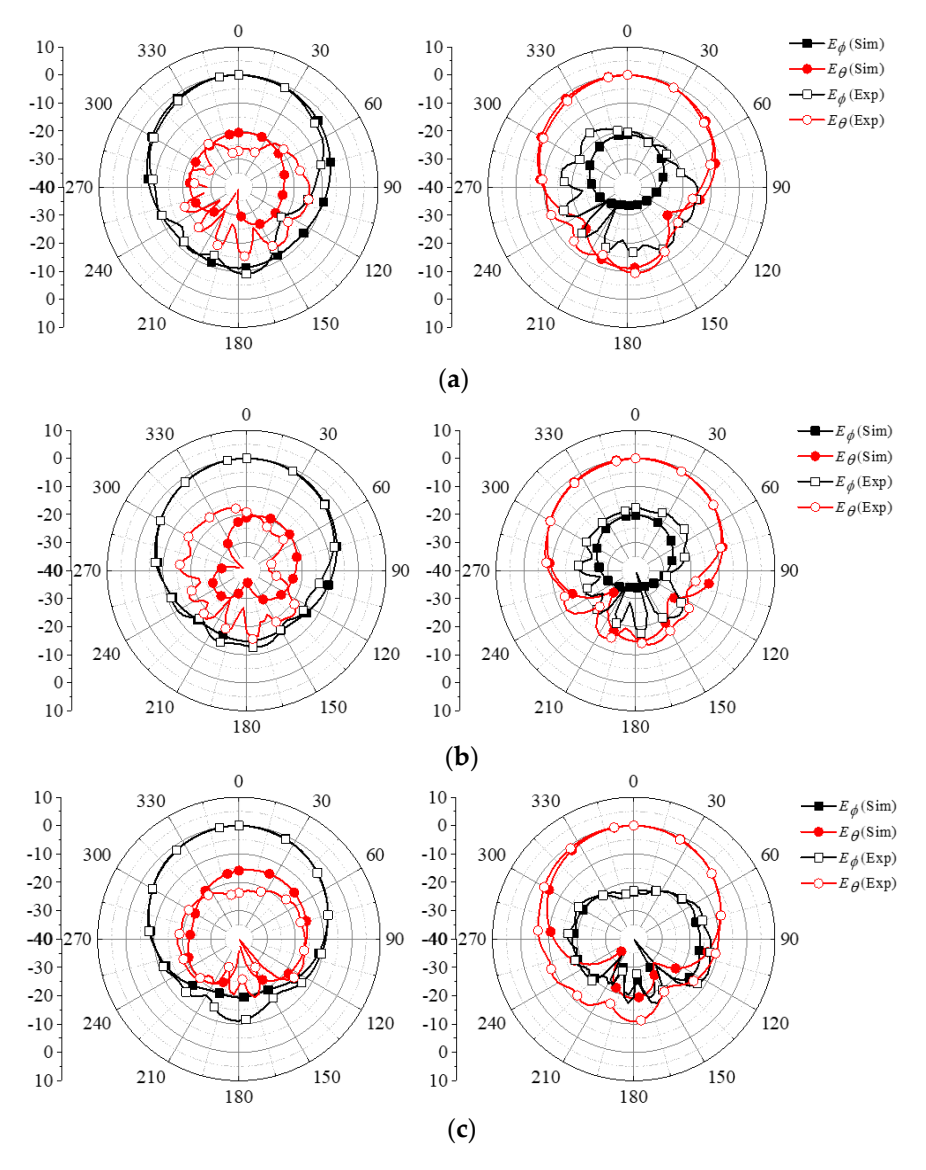


Figure 17. Simulated and measured normalized radiation pattern of $10 \times$ upscaled designed dual-polarized patch antenna with modified L-probe at (a) 2.5, (b) 2.7, and (c) 2.9 GHz.

5. Antenna Performance of Antenna Array

The 5G mmWave application requires high antenna gain to overcome propagation path loss at allocated frequencies. Figure 18 shows various designed 1×4 HLF-PAAs. The antenna arrays are simulated for performance to validate their versatility and effectiveness in various port configurations. The distance of 5 mm between adjacent elements (d) is used for all port configurations.

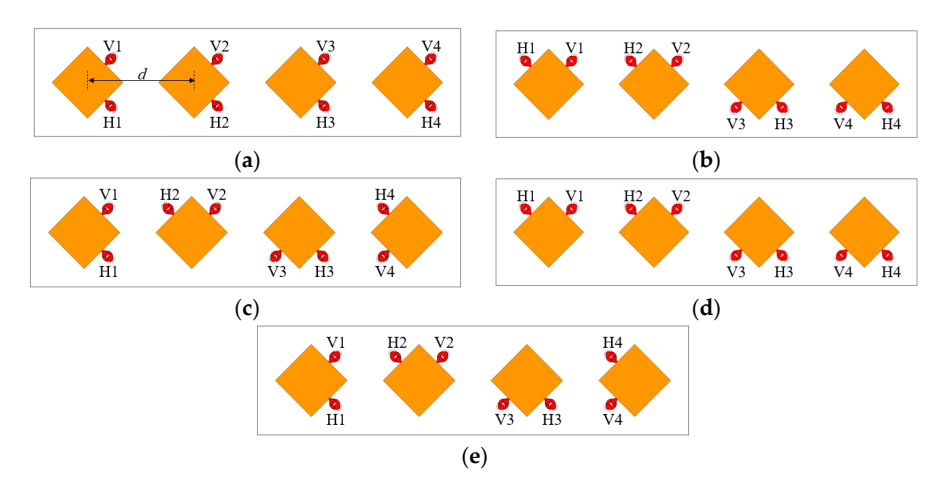


Figure 18. Design of 1×4 designed wideband dual-polarized 5G antenna array with different port configuration: array (a) #1, (b) #2, (c) #3, (d) #4, and (e) #5.

The simulated active S-parameters and S_{21} of the 1×4 HLF-PAA with port configuration #2 and #5 are presented in Figure 19. Other arrays show similar antenna performance and are not presented. A broad -10 dB impedance bandwidth is observed from the simulated S-parameters of HLF-PAA with port configurations #2 and #5, which can cover the low band of 5G NR FR2. The impedance matching is slightly degraded compared to the impedance matching of the optimized unit antenna. This is because the minimum port-to-port isolation is marginally degraded from 18 to 15 dB within the operating frequency in Figure 19b.

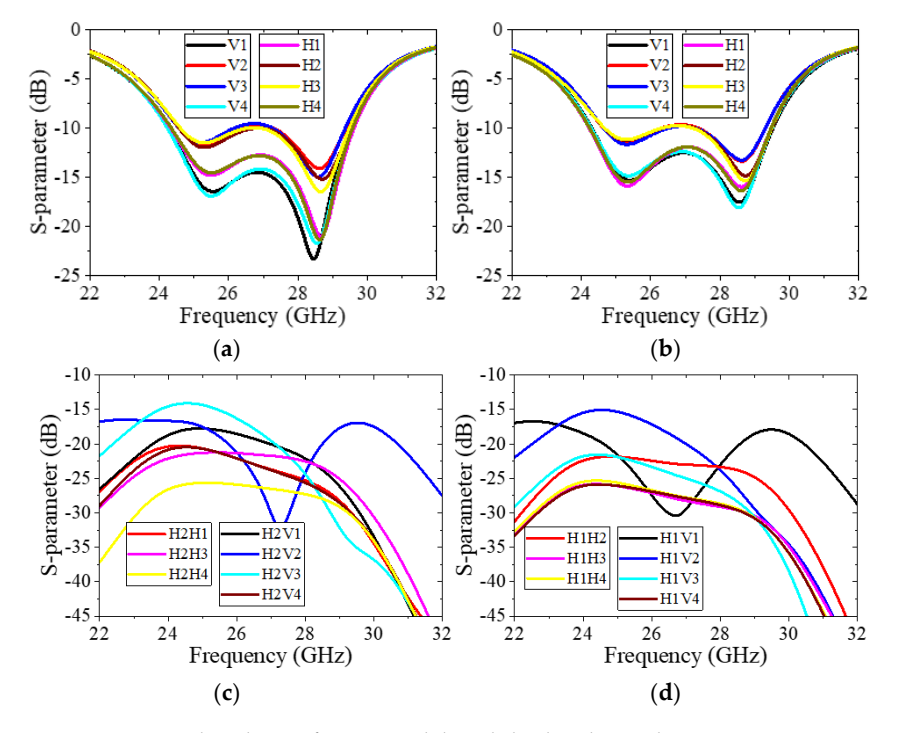


Figure 19. Simulated S_{11} of 1×4 wideband dual-polarized 5G antenna array configuration (**a**) #2 and (**b**) #5 and S_{21} of array (**c**) #2 and (**d**) #5.

The simulated far-field characteristics of the 1×4 HLF-PAA are presented in Figures 20–22. The simulated frequency-dependent RG_{00} of 1×4 HLF-PAAs for all port configurations is shown in Figure 20. The simulated lowest RG_{00} of all HLF-PAAs is 8.5 dBi in the operating frequency bands. The maximum RG_{00} is 10 dBi. Thus, the simulated result demonstrates that the proposed L-probe structures can be used in any array configuration without any significant degradation of bandwidth and isolation. Figure 21 shows the simulated radiation patterns of the developed 1×4 HLF-PAAs with the excitation of V-pol ports in XOZ- and YOZ-plane at 27 GHz. The HLF-PAAs exhibit good broadside radiation at both observation planes.

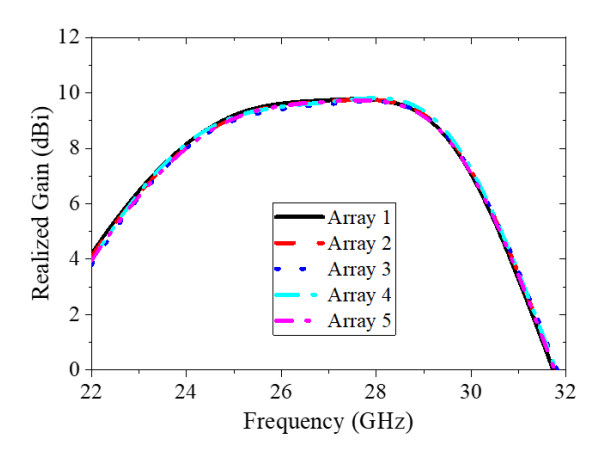


Figure 20. Simulated peak realized gain of 1×4 HLF-PAAs.

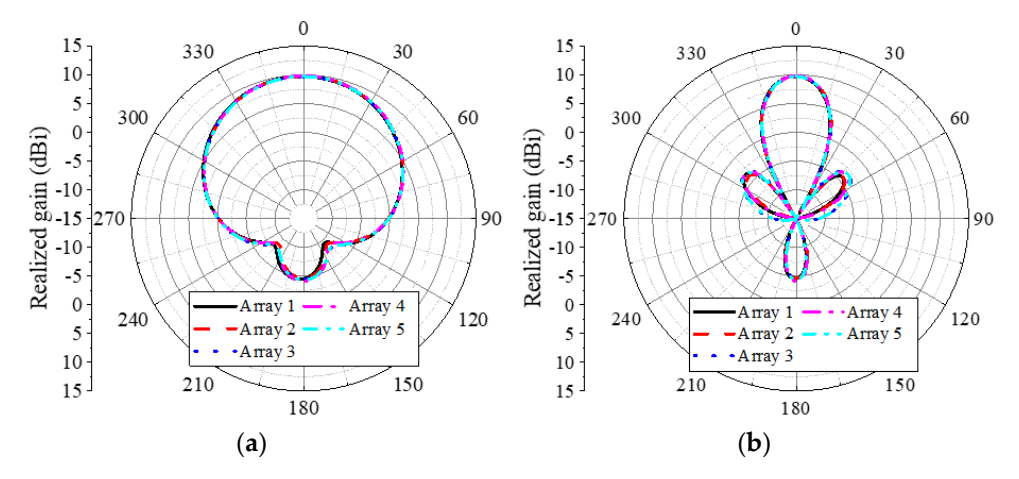


Figure 21. Simulated realized gain radiation pattern of 1×4 HLF-PA arrays at 27 GHz with d of 5 mm: (a) XOZ and (b) YOZ plane.

The beamforming capability of HLF-PAA is validated by varying the phase progression angle from 0° to 120° . The simulated 2D radiation patterns of the HLF-PAA with port configuration #1, when only V-po. ports were excited at 27 GHz, are shown in Figure 22 for the phase progression angle from 0° to 120° . As the angle varies from 0° to 120° , the angle for the maximum gain from the radiation pattern in the YOZ plane was steered from 0° to 318° in Figure 22. Low sidelobe levels (SLLs) less than 9.3 dB are observed. Other HLF-PAAs show the same beamforming capability. It is also noted that the farfield characteristics of the HLF-PAA with the excitation of H-pol. ports show identical performance (not shown here) due to the structural symmetry. Thus, it can be concluded that the developed HLF-PAA is insensitive to the port configuration, which can increase the level of design freedom.

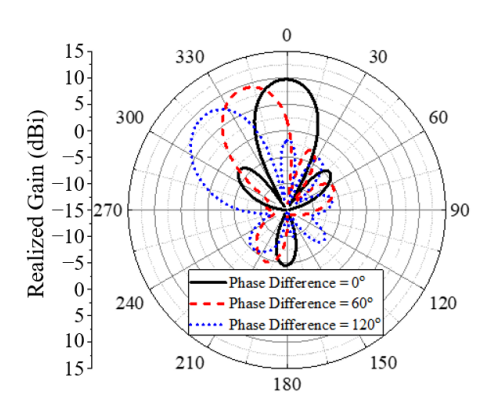


Figure 22. Simulated realized gain radiation pattern of 1×4 HLF-PA array at 27 GHz with d of 5 mm and different phase progression at YOZ planes.

Table 2 summarizes that the designed HLF-PA is compared with previously reported antennas for 5G mmWave applications. The HLF-PA is the only low-cost antenna that shows a wide impedance bandwidth (5.4 GHz: 24.2–29.6 GHz) covering n257, n258, and n261 of the 5G NR FR2, antenna peak gain above 5 dBi, dual polarization, and thickness below 600 μ m, compared to other reported antennas. To emphasize the effectiveness of the proposed antenna, the boxes highlighted in green are antennas that show bandwidth above 20%, gain higher than 5 dBi, a low-cost substrate, thickness below 600 μ m, and the dual-polarization feature, while the boxes highlighted in red are antennas that do not meet the above requirements.

Table 2. Performance comparison between state-of-the-arts and developed antenna *.

Ref.	Frequency Band (-10 dB Bandwidth)	Peak Element Gain	Substrate	Height for Antenna Part	Remark
[2]	30–30.8 GHz (0.8 GHz: 2.6%)	3 dBi	2 HDIs	N. G.	Dual-pol $(S_{ij} > 22 \text{ dB})$
[3]	26.3–30 GHz (3.7 GHz: 13%)	4 dBi	Air cavity and 2 HDIs	N. G.	Dual-pol (S _{ij} : N. G.)
[4]	27.4–29.6 GHz (2.2 GHz: 7.7%)	4.5 dBi	3 HDIs	$490~\mu \mathrm{m}$ (0.045 λ_L)	Dual-pol (S _{ij} : N. G.)
[5]	26.4–29.3 GHz (2.9 GHz: 10%)	N. G.	A6 LTCC	$480~\mu \mathrm{m}$ (0.042 λ_L)	Single-pol (S _{ij} : N. A.)
[6]	22.8–33.3 GHz (10.5 GHz: 37.5%)	N. G.	Organic substrate (HL972LF, GHPL-970LF)	$420~\mu ext{m}$ (0.031 λ_L)	Single-pol (S _{ij} : N. A.)
[9]	26.5–29.5 GHz (3.0 GHz: 11%)	7.4 dBi	TLY-5 and FR-4	1200 μ m (0.11 λ_L)	Dual-pol $(S_{ij} > 23 \text{ dB})$
[11]	22.3–29.6 GHz (7.3 GHz: 28%)	5.8 dBi	TLY-5, FR-27, FR-4, RO4350	2570 μm (0.2 λ_L)	Single-pol (S _{ij} : N. A.)
[14]	24.25–29.5 GHz (5.25 GHz: 20%)	4.5 dBi	RO4003C, RO4450F, TLY-5	$1800~\mu ext{m}$ (0.15 λ_L)	Dual-pol (S _{ij} > 35 dB)
[16]	23-29 GHz (6 GHz: 23.1%)	5 dBi	FR-4, Air	1200 μm (0.092 λ_L)	Dual-pol (S _{ij} > 15 dB)
[18]	27.5–31 GHz (3.5 GHz: 12%)	6 dBi	LTCC	$1183~\mu m$ (0.11 $λ_L$)	Dual-pol (S _{ij} > 14 dB)
[21]	25.87–29.05 GHz (3.18 GHz: 11.5%)	N. G.	RO3003 and RO4003	1100 μ m (0.095 λ_L)	Single-pol (S _{ij} : N. A.)
[22]	26–31.0 GHz (5.0 GHz: 17.5%)	N. G.	Prepreg	$1160~\mu m$ (0.1 λ_L)	Dual-pol $(S_{ij} > 10 \text{ dB})$
[23]	24.2–28.5 GHz (4.3 GHz: 17.8%)	7.5 dBi	EMC, Dielectric polymer	$450~\mu m$ (0.036 λ_L)	Single-pol $(S_{ij} > N. A.)$
This work	24.2–29.6 GHz (5.4 GHz: 20%)	5.1 dBi	FR-4	$600~\mu \mathrm{m}$ (0.048 λ_L)	Dual-pol $(S_{ij} > 18 \text{ dB})$

^{*} N. G.: not given; N. A.: not applicable; λ_L is the air wavelength at lowest frequency.

6. Conclusions

A novel dual-polarized helical-shaped L-probe fed patch antenna (HLF-PA) and phased array (HLF-PAA) were designed to cover n257, n258, and n261 for the 5G new radio (NR) frequency range 2 (FR2). The antenna has a wide impedance bandwidth (>5.4 GHz), excellent isolation between V- and H-ports ($|S_{\rm HV}| > 18$ dB), and good antenna gain (up to 5.1 dBi) with a small height of 600 um for the antenna portion in the antenna-in-package (AiP). The optimized 10× upscaled AiP was fabricated to compare the measured antenna performance with the simulated results. The measured and simulated results show a good agreement. Various 1 × 4 phased arrays were designed based on the optimized single element. The designed 1 × 4 HLF-PAAs showed reasonable isolation between ports ($|S_{ij}| > 15$ dB) and excellent antenna gain with good impedance matching in the desired 5G NR FR2. The developed HLF-PAA has also demonstrated beamforming capabilities, which are vital for 5G wireless communication. Therefore, the designed antenna holds promise in 5G mobile devices.

7. Patents

One U.S. patent entitled "Wideband millimeter (mmWave) antenna" is granted by the U.S. patent office.

Author Contributions: Conceptualization, W.L.; methodology, W.L.; software, W.L. and H.W.; validation, W.L. and H.W.; formal analysis, W.L. and H.W.; investigation, W.L. and H.W.; resources, Y.-K.H.; data curation, W.L. and H.W.; writing—original draft preparation, W.L. and H.W.; writing—review and editing, W.L., H.W., Y.-K.H., M.C. and S.-Y.A.; visualization, H.W.; supervision, Y.-K.H.; project administration, Y.-K.H.; funding acquisition, Y.-K.H. All authors have read and agreed to the published version of the manuscript.

Funding: This work was supported by the NSF under grant number 2137275 and the E. A. "Larry" Drummond Endowment at the University of Alabama.

Data Availability Statement: The data presented in this study are available on request from the corresponding author due to university restrictions.

Conflicts of Interest: Author Woncheol Lee was employed by the company Samsung Electronics. Author Sung-Yong An was employed by the company Samsung Electro-Mechanics Co., Ltd. The remaining authors declare that the research was conducted in the absence of any commercial or financial relationships that could be construed as a potential conflict of interest.

References

- 1. Making 5G NR a Commercial Reality: A Unified, More Capable 5G Air Interface. Available online: https://www.qualcomm.com/media/documents/files/making-5g-nr-a-commercial-reality.pdf (accessed on 6 June 2019).
- 2. Liu, D.; Gu, X.; Baks, C.W.; Valdes-Garcia, A. Antenna-in-Package Design Considerations for Ka-band 5G Communication Applications. *IEEE Trans. Antennas Propag.* **2017**, *65*, 6372–6379. [CrossRef]
- 3. Gu, X.; Liu, D.; Baks, C.; Tageman, O.; Sadhu, B.; Hallin, J.; Rexberg, L.; Valdes-Garcia, A. A Multilayer Organic Package with 64 Dual-polarized Antennas for 28 GHz 5G Communications. In Proceedings of the 2017 IEEE MTT-S International Microwave Symposium (IMS), Honololu, HI, USA, 4–9 June 2017; pp. 1899–1901. [CrossRef]
- 4. Du, J.-K.; So, K.; Ra, Y.; Jung, S.-Y.; Kim, J.; Kim, S.Y.; Woo, S.; Kim, H.-T.; Ho, Y.-C.; Paik, W. Dual-polarized Patch Array Antenna Package for 5G Communication Systems. In Proceedings of the 2017 11th European Conference on Antennas and Propagation (EUCAP), Paris, France, 19–24 March 2017; pp. 3493–3496.
- 5. Mak, C.; Luk, K.; Lee, K.; Chow, Y. Experimental Study of a Microstrip Patch Antenna with L-shaped Probe. *IEEE Trans. Antennas Propag.* **2000**, *48*, 777–783. [CrossRef]
- 6. Xue, M.; Wan, W.; Wang, Q.; Cao, L. Low-profile Wideband Millimeter-wave Antenna-in-Package Suitable for Embedded Organic Substrate Package. *IEEE Trans. Antennas Propag.* **2021**, *69*, 4401–4411. [CrossRef]
- 7. Hazdra, P.; Mazanek, M.; Cermak, J. Wideband Rectangular Microstrip Patch Antenna using L-probe Feeding System. *Radioengineering* **2007**, *16*, 37–41.
- 8. Hong, W.; Baek, K.-H.; Goudelev, A. Grid Assembly-Free 60-GHz Antenna Module Embedded in FR-4 Transceiver Carrier Board. *IEEE Trans. Antennas Propag.* **2013**, *61*, 1573–1580. [CrossRef]
- 9. Kim, W.; Bang, J.; Choi, J. A Cost-effective Antenna-in-Package Design with a 4 × 4 Dual-polarized High Isolation Patch Array for 5G mmWave Applications. *IEEE Access* **2021**, *9*, 163882–163892. [CrossRef]

10. Guo, G.; Wu, L.-S.; Zhang, Y.-P.; Mao, J.-F. Stacked Patch Array in LTCC for 28 GHz Antenna-in-Package Applications. In Proceedings of the 2017 IEEE Electrical Design of Advanced Packaging and Systems Symposium (EDAPS), Haining, China, 14–16 December 2017; pp. 1–3.

- 11. Guo, J.; Hu, Y.; Hong, W. A 45° Polarized Wideband and Wide-Coverage Patch Antenna Array for Millimeter-Wave Communication. *IEEE Trans. Antennas Propag.* **2021**, *70*, 1919–1930. [CrossRef]
- 12. Gu, X.; Liu, D.; Hasegawa, Y.; Masuko, K.; Baks, C.; Suto, Y.; Fujisaku, Y.; Sadhu, B.; Paidimarri, A.; Guan, N.; et al. Antenna-in-Package Integration for a Wideband Scalable 5G Millimeter-Wave Phased-Array Module. *IEEE Microw. Wirel. Compon. Lett.* 2022, 31, 682–684. [CrossRef]
- 13. Seo, J.; Yoon, I.; Jung, J.; Ryoo, J.; Park, J.; Lee, W.; Ko, D.; Oh, J. Miniaturized Dual-Band Broadside/Endfire Antenna-in-Package for 5G Smartphone. *IEEE Trans. Antennas Propag.* **2021**, *69*, 8100–8114. [CrossRef]
- 14. Lu, R.; Yu, C.; Wu, F.; Yu, Z.; Zhu, L.; Zhou, J.; Yan, P.; Hong, W. SIW Cavity-Fed Filtennas for 5G Millimeter-Wave Applications. *IEEE Trans. Antennas Propag.* **2021**, *69*, 5269–5277. [CrossRef]
- 15. Chang, Y.C.; Hsu, C.-C.; Magray, M.I.; Hsu, Y.-C.; Tarng, J.-H. Wideband and Low Profile Miniaturized Magneto-Electric Dipole Antenna for 5G mmWave Applications. In Proceedings of the 2020 IEEE Asia-Pacific Microwave Conference (APMC 2020), Hong Kong, China, 10–13 November 2020.
- 16. Kim, G.; Kim, S. Design and Analysis of Dual Polarized Broadband Microstrip Patch Antenna for 5G mmWave Antenna Module on FR4 Substrate. *IEEE Access* **2021**, *9*, 64306–64316. [CrossRef]
- 17. Park, J.; Choi, D.; Hong, W. Millimeter-wave Phased-array Antenna-in-Package (AiP) using Stamped Metal Process for Enhanced Heat Dissipation. *IEEE Antennas Wirel. Propag. Lett.* **2019**, *18*, 2355–2359. [CrossRef]
- 18. Chou, H.-T.; Chou, S.-J.; Deng, J.D.S.; Chang, C.-H.; Yan, Z.-D. LTCC-based Antenna-in-Package Array for 5G User Equipment with Dual-polarized Endfire Radiations at Millimeter-wave Frequencies. *IEEE Trans. Antennas Propag.* **2021**, *70*, 3076–3081. [CrossRef]
- 19. Yu, B.; Qian, Z.; Lin, C.; Lin, J.; Zhang, Y.; Yang, G.; Luo, Y. A Wideband mmWave Antenna in Fan-Out Wafer Level Packaging With Tall Vertical Interconnects for 5G Wireless Communication. *IEEE Trans. Antennas Propag.* **2021**, *69*, 6906–6911. [CrossRef]
- 20. Li, H.; Li, Y.; Chang, L.; Sun, W.; Qin, X.; Wang, H. A Wideband Dual-Polarized Endfire Antenna Array With Overlapped Apertures and Small Clearance for 5G Millimeter-Wave Applications. *IEEE Trans. Antennas Propag.* **2021**, *69*, 815–824. [CrossRef]
- 21. Zhang, H.; Shamim, A. Wideband and Wide Beam Scanning Dual-Polarized Phased Array Antenna-in-Package Design for 5G Applications. *IEEE Open J. Antennas Propag.* **2024**, *5*, 140–152. [CrossRef]
- 22. Kim, G.; Kim, D.; Lim, K.; Yang, C.; You, C.; Kim, S. Dual-band Dual-polaried Rhombic Patch Antenna Array for 5G mmWave RF Front End Antenna-in-Package Module. *IEEE Antennas Wirel. Propag. Lett.* **2024**, 23, 2120–2124. [CrossRef]
- 23. Yin, Y.; Xia, C.; Liu, S.; Zhang, Z.; Chen, C.; Wang, G.; Wang, C.; Wu, Y. Ultrathin Antenna-in-Package Based on TMV-Embedded FOWLP for 5G mm-Wave Applications. *Electronics* **2024**, *13*, 839. [CrossRef]

Disclaimer/Publisher's Note: The statements, opinions and data contained in all publications are solely those of the individual author(s) and contributor(s) and not of MDPI and/or the editor(s). MDPI and/or the editor(s) disclaim responsibility for any injury to people or property resulting from any ideas, methods, instructions or products referred to in the content.